

Model of Calcium Oscillations Due to Negative Feedback in Olfactory Cilia

J. Reidl,* P. Borowski,[†] A. Sensse,[‡] J. Starke,* M. Zapotocky,[†] and M. Eiswirth[‡]

*Institute of Applied Mathematics, University of Heidelberg, and WIN-Research Group of Olfactory Dynamics, Heidelberg Academy of Science and Humanities, Heidelberg, Germany; [†]Max Planck Institute for the Physics of Complex Systems, Dresden, Germany; and [‡]Fritz-Haber-Institute of the Max Planck Society, Berlin, Germany

ABSTRACT We present a mathematical model for calcium oscillations in the cilia of olfactory sensory neurons. The underlying mechanism is based on direct negative regulation of cyclic nucleotide-gated channels by calcium/calmodulin and does not require any autocatalysis such as calcium-induced calcium release. The model is in quantitative agreement with available experimental data, both with respect to oscillations and to fast adaptation. We give predictions for the ranges of parameters in which oscillations should be observable. Relevance of the model to calcium oscillations in other systems is discussed.

INTRODUCTION

Oscillations in intracellular calcium occur under a variety of conditions and play functional roles in signal transduction and cell regulation (1). They typically arise from calcium-induced calcium release (CICR) mechanisms, in which an increase in cytoplasmic calcium level leads to increased Ca^{2+} influx from intracellular Ca^{2+} stores (2). Such positive feedback is implemented, e.g., through the regulation by Ca^{2+} of the Ca^{2+} -permeable IP_3 and ryanodine receptor channels of the endoplasmic reticulum (1).

Calcium oscillations arising from negative feedback have received much less attention. A notable exception is the case of coupled calcium and cyclic AMP oscillations. A mathematical analysis of conditions under which cAMP-induced Ca^{2+} influx coupled to Ca^{2+} -modulated cAMP production leads to oscillations was given in Rapp and Berridge (3). A specific mechanism of this type was proposed in Cooper et al. (4), in which Ca^{2+} enters the cell through cyclic-nucleotide-gated (CNG) channels and Ca^{2+} is assumed to cooperatively suppress the activity of adenylyl cyclase. Oscillations in cAMP that arise from coupling to Ca^{2+} oscillations were recently reported in embryonic spinal neurons (5); in this case, however, the Ca^{2+} oscillations are due to a CICR mechanism and do not require varying cAMP. To the best of our knowledge, strictly mutually dependent oscillations of Ca^{2+} and cAMP, in which they are both essential (6,7), have not been conclusively observed.

The coupling of cyclic nucleotide dynamics to Ca^{2+} influx through CNG channels forms the basis of sensory signal transduction in vertebrate olfactory sensory neurons (8). Pronounced oscillations of the Ca^{2+} level in the cilia of olfactory sensory neurons were recently reported by Reisert and Matthews (9). In addition, oscillations in receptor current presumed to be indicative of Ca^{2+} oscillations were observed in Frings and Lindemann (10), Reisert and Matthews (11,12),

and Suzuki et al. (13). It was argued in Reisert and Matthews (11) and Suzuki et al. (13) that the observed oscillations are probably due to the mechanism proposed in Cooper et al. (4). The corresponding cAMP oscillations have not, however, so far been confirmed experimentally. In addition, Ca^{2+} regulation of adenylyl cyclase in olfactory sensory neurons occurs on a timescale of minutes (14), whereas the period of Ca^{2+} oscillations is of the order of seconds.

In this article, we propose a mechanism for Ca^{2+} oscillations in olfactory sensory neurons that depends neither on cAMP variations nor on calcium-induced calcium release. The mechanism is based on direct negative regulation of CNG channels by calcium/calmodulin. This form of negative feedback is well established in olfactory sensory neurons (15,16), is known to play the key role in fast olfactory adaptation (17,18), and has been analyzed in detail biochemically (16,19,20). Using parameter values inferred from Bradley et al. (19), Munger et al. (20), Schild and Restrepo (21), and Reisert et al. (22), we construct a mathematical model of the coupled kinetics of calcium, calmodulin, and CNG channels. We then show that our model predicts persistent oscillations of Ca^{2+} for rate constants and concentrations in the physiological range and correctly captures fast adaptation (≈ 1 s).

This article is organized as follows: in “Signal Transduction in Olfactory Cilia”, we review some relevant facts about olfactory response. “Source of Instability and Hopf Bifurcation” suggests a biochemical mechanism and presents an analytical proof of the existence of oscillations using the formalism of stoichiometric network analysis. In the following section, we develop and numerically analyze a detailed kinetic model. We show that the model is in good agreement with available data and make predictions for the ranges of odorant concentration, calmodulin concentration, and system size in which Ca^{2+} oscillations should be observable. The relation of our model to other mechanisms of biochemical oscillations, as well as the limits of the validity of our model, are detailed in “Discussion”.

Submitted January 18, 2005, and accepted for publication October 6, 2005.

Address reprint requests to Jens Starke, Tel.: 49-6221-548980; E-mail: starke@iwr.uni-heidelberg.de.

© 2006 by the Biophysical Society

0006-3495/06/02/1147/09 \$2.00

doi: 10.1529/biophysj.104.058545

SIGNAL TRANSDUCTION IN OLFACTORY CILIA

The detection of odorants takes place in the cilia of olfactory sensory neurons. The signal transduction pathway has been studied in detail in a variety of species and is particularly well understood in vertebrates (reviewed in (21)), where the concentration of odorant molecules outside of the cilium is transduced into a change of the level of the second messenger cAMP inside the cilium, leading to the opening of CNG-gated ion channels and the influx of Ca^{2+} (see Fig. 1 and its caption). Subsequently, the opening of Ca^{2+} -gated chloride channels results in depolarization of the cilium that is sufficient to trigger the generation of action potentials in the soma of the sensory neuron.

In addition to being part of the direct forward path of the signal, Ca^{2+} has been shown to play a key role in adaptation of the olfactory response (reviewed in (23)). Several Ca^{2+} -dependent negative feedback mechanisms have been identified: increase in the closing rate of the CNG channel; increase in PDE activity; and activation of CaMKII leading to decrease in adenylyl cyclase activity (see Fig. 1). These feedback mechanisms are expected to act simultaneously following the exposure to a strong odorant signal, and their relative importance is currently under debate.

In the following we concentrate on the CaM4-mediated closing of channels (direct feedback), before addressing its possible interaction with other feedback loops in the discussion.

SOURCE OF INSTABILITY AND HOPF BIFURCATION

When studying a model it is generally helpful to check which types of dynamical behavior are to be expected using analytical techniques before carrying out numerical calculations. We use stoichiometric network analysis (SNA) (24) to check analytically whether the system of Fig. 1 can give rise

to oscillations (for details of the procedure, see (31,32); for an accessible introduction to SNA, see (25,26); for a computational package, see (27,28); for recent developments in SNA, see (29,30)). The decisive advantage of the SNA formalism is that the complete set of steady states can be explicitly written down and their stability analyzed, therefore revealing the presence (or absence) of local bifurcations anywhere in the parameter space. In SNA the rate constants of the reactions and the concentrations at stationary points do not appear explicitly, i.e., can be left unspecified. The procedure of SNA allows for a substantial simplification of the bifurcation analysis and hence for fast checks of the qualitative dynamical behavior inherent in the reaction schemes. Nevertheless, it should be noted that the following SNA gives only existence results and for quantitative results, further knowledge of the rate constants is necessary.

In SNA, a reaction mechanism of n species and r reactions is completely specified by two $n \times r$ matrices: the stoichiometric matrix ν , which contains the (positive or negative) stoichiometric change of each species in each reaction; and the kinetic matrix κ , which contains the respective kinetic exponents, assuming that the kinetics of the j^{th} reaction is given (or can be approximated) by power laws $k_j \prod_i x_i^{\kappa_{ij}}$, where x_i denotes the concentration of the i^{th} species. For ease of visualization in network diagrams, ν is scaled so that it consists of small integers. All the rate constants k_j are assumed to be able to take on any nonnegative value (complete parameter set (33)).

The elements of ν and κ can be written down explicitly or encoded in a network diagram (see Fig. 2). Thus, Fig. 2 A represents the part of Fig. 1 that contains the direct feedback (shown there with *thick arrows*) and is equivalent to the reaction scheme analyzed numerically in “Kinetic Model and Numerical Analysis” (i.e., encodes the stoichiometry and assumptions about kinetic exponents). Inspection of Fig. 2 A reveals that there are no autocatalytic loops (24,25,31,34) that could give rise to an instability; instead, the negative three-loop of CNG^0 —causing the influx of Ca^{2+} producing

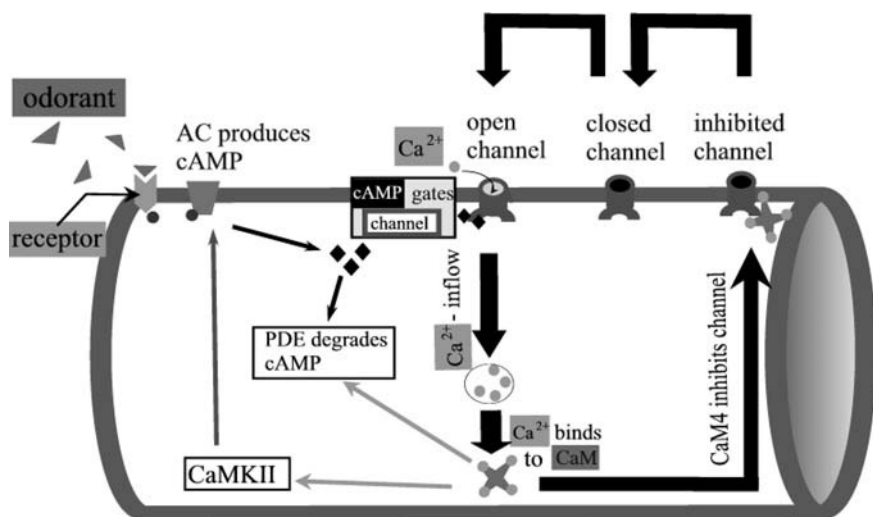


FIGURE 1 Signal transduction in olfactory cilia. Odorant binding to the receptor results in production of cAMP, which in turn activates the CNG channels. Calmodulin (CaM) reacts with the incoming Ca^{2+} to CaM4, which inhibits the channels, resulting in a negative feedback (*thick arrows*). Other feedbacks include the enhancement of phosphodiesterase (PDE) activity by CaM4 and the CaM4-mediated activation of the kinase CaMKII, which reduces the cAMP production (*thin arrows*). In the text, we denote the nongated (*closed*), cAMP-gated (*open*), and CaM4-gated (*inhibited*) channels as CNG^c , CNG^o , and CNG^i , respectively.

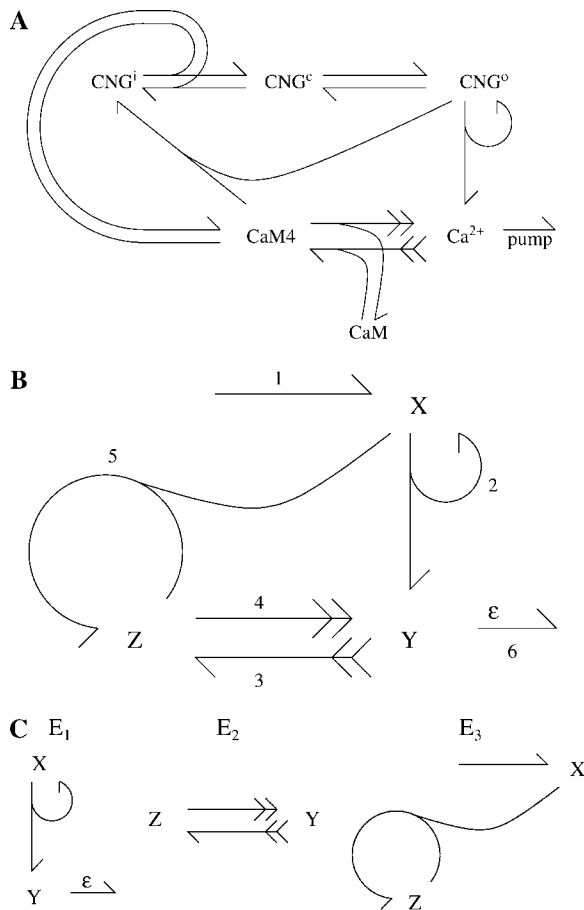


FIGURE 2 Network diagrams describing the relevant part of olfactory signal transduction. (A) Direct feedback model; (B) reduced version of panel A retaining only relevant feedback loop. Note that CaM4 (denoted Z) is now directly reproduced in the reaction with CNG^o (X), since, in addition to CNG^c, the intermediate species CNGⁱ has been eliminated. (C) Extreme subnetworks of network in panel B. The species symbols are connected by arrows denoting the reactions. The (positive) stoichiometric coefficients of products are given by the number of barbs on the arrow, and the (negative) ones of reactants are presented by the total number of feathers, whereas the kinetic exponent of a reactant is symbolized by the number of left feathers (e.g., the formation of CaM4 requires four Ca²⁺ ions, the kinetics is assumed second-order, so two out of four feathers are put on the left). By convention, no feathers are shown if stoichiometric and kinetic coefficients are both unity (24,25). The small kinetic exponent for the Ca²⁺ pump is denoted by ϵ .

CaM4, which in turn blocks CNG^o—is the only possible source of instability (35). We therefore examine a radically reduced network where only these three species and their six reactions are retained (Fig. 2 B). The reduced network no longer contains CNGⁱ and CNG^c. Denoting the concentration of open channels by X, of Ca²⁺ by Y, and of CaM4 by Z, the kinetic equations are

$$\begin{aligned} \frac{d}{dt}X &= k_1 - k_5XZ \\ \frac{d}{dt}Y &= k_2X - 4k_3Y^2 + 4k_4Z - k_6Y^\epsilon \\ \frac{d}{dt}Z &= k_3Y^2 - k_4Z. \end{aligned} \quad (1)$$

We have replaced the four-step formation of CaM4 out of CaM by one effective reaction of second order in [Ca²⁺] (the term $-4k_3Y^2$ in Eq. 1). This is expected to be a good approximation since there are two sets of sites, each set composed of two highly cooperative binding sites (36). The term $-k_6Y^\epsilon$ with effective exponent ϵ corresponds to extrusion of Ca²⁺ from the cilium by pumps and exchangers. In matrix form, Eq. 1 can be expressed as

$$\frac{d}{dt}\vec{x} = \nu\vec{v}, \quad (2)$$

where $\vec{x} = (X, Y, Z)^T$ is the vector of concentrations of the three species,

$$\nu = \begin{pmatrix} 1 & 0 & 0 & 0 & -1 & 0 \\ 0 & 1 & -4 & 4 & 0 & -1 \\ 0 & 0 & 1 & -1 & 0 & 0 \end{pmatrix} \quad (3)$$

is the matrix of stoichiometric coefficients, and $\vec{v} = (k_1, k_2X, k_3Y^2, k_4Z, k_5XZ, k_6Y^\epsilon)^T$ is the vector of velocities of the six reactions. The reaction vector can be written as

$$v_j = k_j \prod_i x_i^{\kappa_{ij}}, \quad (4)$$

where

$$\kappa = (\kappa_{ij}) = \begin{pmatrix} 0 & 1 & 0 & 0 & 1 & 0 \\ 0 & 0 & 2 & 0 & 0 & \epsilon \\ 0 & 0 & 0 & 1 & 1 & 0 \end{pmatrix} \quad (5)$$

is the matrix of kinetic exponents, $i = 1 \dots n$ labels the species, and $j = 1 \dots r$ labels the reactions. In general, a reaction mechanism is completely specified by the two $n \times r$ matrices ν and κ . For the model specified by Eqs. 3 and 5 we first give the representation of its set of stationary states in SNA and then carry out its bifurcation analysis.

Set of stationary states

In SNA, the complete set of stationary states can be written down in closed form as all linear combinations, $\sum_j j_i \vec{E}_i$, with nonnegative coefficients j_i of a certain number of undecomposable subnetworks \vec{E}_i (also referred to as extreme currents, basic feasible solutions, stationary flows, stoichiometric generators) (33). For the network of Fig. 2 B (with six reactions and three species), there are three such irreducible subnetworks ($\vec{E}_1, \vec{E}_2, \vec{E}_3$), which are shown in Fig. 2 C. These are the smallest subnetworks that still fulfill the stationary state condition that the production rates equal the degradation rates for all species of this subnetwork. In the language of the network diagrams, this means that for all vertices (species) the inflows are equal to the outflows, i.e., the number of (incoming) barbs and (outgoing) feathers are equal for every species.

For the first subnetwork \vec{E}_1 , the Ca²⁺ inflow $v_2 = k_2X$ through open CNG channels is balanced by the outflow through the pumps $v_6 = k_6Y^\epsilon$, and all other reaction velocities

are set to zero. This gives a stationary state with velocity vector $\vec{v} = j_1 \vec{E}_1$, where $j_1 \equiv v_2 = v_6$ and $\vec{E}_1 = (0, 1, 0, 0, 0, 1)^T$. Likewise, in the second subnetwork \vec{E}_2 , when $\vec{v} = j_2 \vec{E}_2$ with $\vec{E}_2 = (0, 0, 1, 1, 0, 0)^T$, the production and degradation rates compensate each other for both species, Ca^{2+} and CaM4 . The remaining reactions r_1 and r_5 generate the last subnetwork $\vec{E}_3 = (1, 0, 0, 0, 1, 0)^T$. From linear algebra it follows that the complete set of subnetworks forms a basis of the right null space of the stoichiometric matrix ν , i.e., every velocity vector \vec{v} fulfilling the condition of stationarity $(d)/(dt)\vec{x} = \nu\vec{v} = \vec{0}$ is a linear combination of the extreme currents: $\vec{v} = \sum_k j_k \vec{E}_k$. The coefficients j_k are nonnegative (i.e., \vec{v} forms a convex cone) because only the intersection with the nonnegative orthant are physically meaningful stationary states.

The Jacobian of the dynamical system (Eqs. 2 and 4) can be calculated as $J = \nu \text{diag}(\sum_k j_k \vec{E}_k) \kappa^T \text{diag}(\vec{x}_0)^{-1}$, where $\text{diag}(\vec{u})$ is defined as the diagonal matrix with the components of \vec{u} as diagonal entries and \vec{x}_0 is the vector of stationary concentrations. Since the multiplication with the positive stationary concentrations $\text{diag}(\vec{x}_0)$ does not change the sign pattern of the Jacobian (24), it is often (as in our case) sufficient to analyze the stability properties of the reduced Jacobian: $\tilde{J} = \nu \text{diag}(\sum_k j_k \vec{E}_k) \kappa^T$. In this manner, the bifurcation analysis of the investigated model with six undetermined rate constants is reduced to depend on the three flux coefficients j_1 , j_2 , and j_3 . As scaling these parameters by a common positive factor does not change stability, we can choose $j_2 = 1$, and are left with only two free parameters.

Occurrence of Hopf bifurcation

A necessary and sufficient condition for the occurrence of a Hopf bifurcation (based on a modified Routh scheme; see Clarke (25)) has been given in Eiswirth et al. (32). Essentially it arranges the sums a_i over all principal minors α_i of a given order i of the Jacobian J or \tilde{J} (i.e., the coefficients a_i of the respective characteristic polynomial) in two rows and computes the elements of the further rows in a way analogous to 2×2 determinants.

For a system with three species, the characteristic polynomial is $p_J(\lambda) = \lambda^3 + a_1\lambda^2 + a_2\lambda + a_3$ and the scheme becomes as shown in Table 1; see below.

A Hopf bifurcation occurs if the last two nonzero entries in the first column change sign simultaneously—obviously the case if $a_1a_2 - a_3$ does. For all other kinds of changes from stability to instability $a_3 = \det(\tilde{J})$ would have to change the sign.

TABLE 1

1	a_2	0
a_1	a_3	0
$a_1a_2 - a_3$	0	–
$(a_1a_2 - a_3)a_3$	0	–
0	–	–

Using this procedure, we now examine the stability of the steady state with velocity vector $j_1\vec{E}_1 + \vec{E}_2 + j_3\vec{E}_3$, treating the as-yet-unspecified exponent ε (see Fig. 2) as an additional parameter. Evaluation of the sums over the minors results in $a_1 = 9 + j_1\varepsilon + j_3$; $a_2 = 9j_3 + j_1\varepsilon + j_1j_3\varepsilon$; and $a_3 = 2j_1j_3 + j_1j_3\varepsilon$.

Since a_3 is always positive, the only possibility of local loss of stability is via a Hopf bifurcation. In addition, no saddle-node bifurcation can occur since a_3 cannot change sign; actually, this conclusion already follows from the absence of autocatalytic loops. To linear order in ε , the system becomes oscillatory for $a_1a_2 - a_3 = 81j_3 + 9j_3^2 + \varepsilon(j_1j_3^2 + 9j_1 + 18j_1j_3) - 2j_1j_3 < 0$. This condition can readily be fulfilled for $j_1 \gg j_3 \gg \varepsilon$, i.e., when \vec{E}_1 carries considerably higher weight than the other subnetworks (meaning the rates of the reactions in \vec{E}_1 must be large), and the kinetic exponent ε is sufficiently small. The inequality $j_1 \gg j_3$ is always satisfied: in terms of the rate constants of Table 2 we get $j_1/j_3 \approx i_{\text{Ca}}/(k_{\text{CNG}_2}^+ [\text{CAM}^{\text{tot}}]) \approx 10^3$.

Ca^{2+} is pumped out of the cell; near pump saturation, such a process is of very low order in $[\text{Ca}^{2+}]$. Actually, no Hopf bifurcation could be numerically found for ε above ~ 0.05 (the exact value depending on the other parameters). Therefore, Ca^{2+} has to reach concentrations at or near pump saturation so that oscillations can occur. In contrast, the kinetic order of Ca^{2+} in the formation of CaM4 was uncritical, i.e., the existence of oscillations was robust using kinetic exponents of 1 or even 4.

Such analytical considerations not only showed what bifurcations to look for, but also proved very helpful in determining the range of parameters for subsequent numerical studies.

KINETIC MODEL AND NUMERICAL ANALYSIS

Our full model (see Fig. 2 A) includes the following reactions: channel gating by cAMP (the opening rate k_{act}^+ in Eq. 6 increases with cAMP, which in turn depends on odorant concentration); Ca^{2+} binding to calmodulin in Eq. 7; irreversible binding of Ca^{2+} /calmodulin (CaM4) to open channels in Eq. 8; and reversible binding of CaM4 to closed channels in Eq. 9,

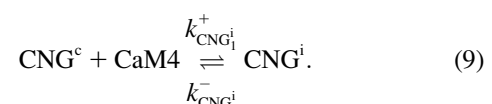
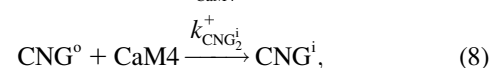
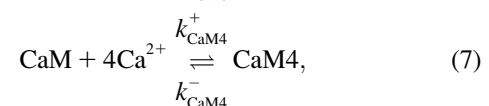
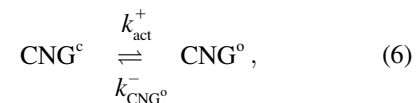


TABLE 2 Parameters used in the model

Parameter	Unit	Value	Literature
σ	dm	5×10^{-7}	$(2.5 \dots 6.3) \times 10^{-7}$ (21).*
$[\text{CNG}^{\text{tot}}]_s$	(mol/dm ²)	1.3×10^{-13}	1.3×10^{-13} (22) (rat); 1.2×10^{-12} (53) (frog).
$[\text{CaM}^{\text{tot}}]$	(mol/dm ³)	2×10^{-5}	10^{-5} (54).
$k_{\text{CNG}^0}^-$	(1/s)	10^{-2}	Very slow (19) Fig. 1 A (<i>inset</i>). [†]
k_{CaM4}^-	(1/s)	2.5	10. . . 40 (36) [‡] ; slow (20) Fig. 3 B.
k_{CaM4}^+	(1/s)(dm ⁶ /mol ²)	1.1×10^9	“too fast to be measured” (36). [§]
$k_{\text{CNG}_1^i}^+$	(1/s) (dm ³ /mol)	2.1×10^6	1.7×10^7 (19) Fig. 3 D [¶] ; 1.5×10^6 (20).
$k_{\text{CNG}_2^i}^+$	(1/s)(dm ³ /mol)	2.1×10^6	$= k_{\text{CNG}_1^i}^+$ (19).
$k_{\text{CNG}_1^i}^-$	(1/s)	3.4×10^{-1}	$> 2.2 \times 10^{-1}$ (20). ^{**}
i_{Ca}	(1/s)	2×10^4	7.8×10^4 (22).
k_{Ca}	(1/s)(mol/dm ²)	10^{-10}	See text.
K_{Ca}	(mol/dm ³)	1.2×10^{-7}	See text.
k_{act}^+	(1/s)	Rest. state: 1.6×10^{-5} (corresponds to $[\text{Ca}^{2+}] = 5 \times 10^{-9}$ (mol/dm ³)) Oscill.: 5.5×10^{-2} Adapt.: 5.5	5×10^{-8} (21). See text. See text.

*Volume/area ratio for a cylinder of diameter 0.1 . . . 0.25 μm .

[†]Assuming PDE destroys remaining cAMP fast.

[‡]Slowest rate in the cooperative binding of the four Ca^{2+} .

[§]Our value is an order-of-magnitude estimate based on the dissociation constants for the four binding sites given in Cohen and Klee (36), Delville et al. (50), and our value for k_{CaM4}^- .

[¶]Assuming CNGA2A4B1b is equivalent to native CNG.

^{||}Estimated from τ_1 in Fig. 3 D of Munger et al. (20).

^{**}Estimated from τ for + / + in Fig. 3 E of Munger et al. (20) assuming fast opening of CNG^c .

In addition, there is a Ca^{2+} influx proportional to the number of channels in the open state CNG^0 , and Ca^{2+} is actively pumped out.

The system contains two conservation constraints, so that only four of the six species are independent:

$$[\text{CNG}^{\text{tot}}]_s = [\text{CNG}^c]_s + [\text{CNG}^0]_s + [\text{CNG}^i]_s, \quad (10)$$

$$[\text{CaM}^{\text{tot}}] = [\text{CaM}] + [\text{CaM4}] + \frac{1}{\sigma}[\text{CNG}^i]_s. \quad (11)$$

Square brackets with a subscript s denote surface, others volume concentrations. When volume species are produced by surface species or vice versa, the concentrations have to be converted at the respective location by division or multiplication by σ , which represents the thickness of the cytoplasmic layer in cilia. More generally we define σ as the ratio of cytoplasmic volume to membrane area; for a cylinder of diameter d , we get $\sigma = d/4$. Taking into account Eqs. 10 and 11, the reaction Eqs. 6–9 lead to four coupled ordinary differential equations for the concentrations of open channels, internal calcium, calcium-loaded calmodulin, and channels that bind calmodulin:

$$\begin{aligned} \frac{d}{dt}[\text{CNG}^0]_s &= k_{\text{act}}^+([\text{CNG}^{\text{tot}}]_s - [\text{CNG}^0]_s - [\text{CNG}^i]_s) \\ &\quad - k_{\text{CNG}^0}^-[\text{CNG}^0]_s - k_{\text{CNG}_2^i}^+[\text{CNG}^0]_s[\text{CaM4}], \end{aligned} \quad (12)$$

$$\begin{aligned} \frac{d}{dt}[\text{Ca}^{2+}] &= \frac{1}{\sigma}i_{\text{Ca}}[\text{CNG}^0]_s - \frac{1}{\sigma}k_{\text{Ca}}\frac{[\text{Ca}^{2+}]}{[\text{Ca}^{2+}] + K_{\text{Ca}}} \\ &\quad - 4k_{\text{CaM4}}^+[\text{Ca}^{2+}]^2\left([\text{CaM}^{\text{tot}}] - [\text{CaM4}] - \frac{1}{\sigma}[\text{CNG}^i]_s\right) \\ &\quad + 4k_{\text{CaM4}}^-[\text{CaM4}], \end{aligned} \quad (13)$$

$$\begin{aligned} \frac{d}{dt}[\text{CaM4}] &= k_{\text{CaM4}}^+[\text{Ca}^{2+}]^2\left([\text{CaM}^{\text{tot}}] - [\text{CaM4}] - \frac{1}{\sigma}[\text{CNG}^i]_s\right) \\ &\quad - k_{\text{CaM4}}^-[\text{CaM4}] - \frac{1}{\sigma}k_{\text{CNG}_1^i}^+[\text{CaM4}](\text{CNG}^{\text{tot}}]_s - [\text{CNG}^0]_s \\ &\quad - [\text{CNG}^i]_s) + \frac{1}{\sigma}k_{\text{CNG}_1^i}^-[\text{CNG}^i]_s - \frac{1}{\sigma}k_{\text{CNG}_2^i}^+[\text{CaM4}][\text{CNG}^0]_s, \end{aligned} \quad (14)$$

$$\begin{aligned} \frac{d}{dt}[\text{CNG}^i]_s &= k_{\text{CNG}_1^i}^+[\text{CaM4}](\text{CNG}^{\text{tot}}]_s - [\text{CNG}^0]_s - [\text{CNG}^i]_s) \\ &\quad - k_{\text{CNG}_1^i}^-[\text{CNG}^i]_s + k_{\text{CNG}_2^i}^+[\text{CaM4}][\text{CNG}^0]_s. \end{aligned} \quad (15)$$

Most terms are described by mass-action kinetics, CaM4 formation being of second order in $[\text{Ca}^{2+}]$ (see “Source of Instability and Hopf Bifurcation”). In Eq. 13, a constant Ca^{2+} -current through an open CNG channel is assumed, and calcium extrusion is modeled by a Hill type equation that effectively represents the summed effect of both calcium pumps and Na/Ca exchangers. (The Ca^{2+} extrusion rates depend sensitively on membrane voltage and concentrations of other ion species (Na, K). Corresponding quantitative information is presently not available for olfactory cilia (22), therefore it is currently not possible to construct a mechanistically justified expression for Ca extrusion.) The coupled differential equations were solved numerically with a stiff solver using the parameter values given in Table 2. An alternative parameter set that leads to similar numerical results is presented in Appendix A.

We first verified that our model correctly captures the adaptation of olfactory response as seen in the experiments of Leinders-Zufall et al. (37). The odorant pulse is

represented in the simulation by increasing k_{act}^+ from an assumed resting value of $1.6 \times 10^{-5} (1/\text{s})$ to $5.5 (1/\text{s})$ for a period of 100 ms. The first pulse is presented at 0 s, the second after a time interval of 2 s, 4 s, 6 s, 8 s, 10 s, or 12 s, respectively. Shown in Fig. 3 A are the time courses of Ca^{2+} concentrations superimposed for these six different runs. For a better understanding of the underlying mechanism, the simulated time evolution of the concentrations of all species are shown in Fig. 3 B. The stimulus presentation is followed by the opening of CNG channels and rapid accumulation of Ca^{2+} . The $100\text{-}\mu\text{M}$ concentration of Ca^{2+} reached in our simulation is consistent with levels up to $500\text{ }\mu\text{M}$ predicted by a detailed biophysical model of the steady state of a fully activated cilium in Lindemann (38). Within 400 ms, CaM4 (dotted curve in Fig. 3 B) reaches levels sufficient to fully inhibit the channels (thin solid curve) and therefore to reduce the open channel fraction (thick solid curve) to zero level. The saturation of the Ca^{2+} pump rate is reflected in the

subsequent slow (almost linear) decay of Ca^{2+} concentration, completed within 1 s of the stimulus. The slowest process is the disinhibition of CNG channels (10). Most channels are still inhibited (thin solid curve) when the second pulse is presented at $t = 4$ s, resulting in a reduced response.

The time for recovery from adaptation is consistent with the experimental data of Fig. 8 A in Leinders-Zufall et al. (37), which is reprinted in Fig. 3 A. Our model also reproduces the results of double pulse experiments in Fig. 2, D–F, of Munger et al. (20). The shift in the onset of the Ca^{2+} peaks in the experiment compared to the simulation (Fig. 3) corresponds to the time delay between the application of odorant and the increase in cAMP concentration. The corresponding part of the signaling pathway is not included in our model.

We now model the experiments of Reiser and Matthews (9) in which the odorant was presented for a prolonged period and the intracellular Ca^{2+} concentration was measured directly. We keep all parameter values (except k_{act}^+) the same as above for the double-pulse experiments. To choose the appropriate value of k_{act}^+ we assume a linear relation between the concentrations of odorant and cAMP, and a quadratic relation between that of cAMP and k_{act}^+ (39).

As the concentration of odorant (cineole) used in this experiment was 1/10 of the concentration in the double-pulse experiment of Leinders-Zufall et al. (37), we choose $k_{\text{act}}^+ = 5.5 \times 10^{-2} (1/\text{s})$. Our model then produces calcium oscillations with a period of 2.5 s (Fig. 4 A), in good agreement with the data in Fig. 5 A of Reiser and Matthews (9), which is reprinted in Fig. 4 A. During these oscillations, the concentrations of open channels, internal Ca^{2+} , CaM4, and inhibited channels reach their maximal values (Fig. 4 B) in the same order as in the double-pulse experiments. Throughout the oscillations, however, inhibition is never complete, and the open fraction remains above 0.02. The horizontal dashed line in Fig. 4 B indicates the open fraction $k_{\text{Ca}}/(i_{\text{Ca}}[\text{CNG}^{\text{tot}}]) = 0.039$ at which the pumps are no longer able to compensate the influx through channels, leading to rapid accumulation of Ca^{2+} . It is notable that the oscillations in the inhibited fraction (thin solid curve in Fig. 4 B) and in Ca^{2+} concentration (dashed curve) run almost in antiphase (maximum in inhibition coincides with minimum in Ca^{2+} concentration). Consequently, the oscillations are not damped out. Oscillations with increased period are obtained when the rate of Ca^{2+} extrusion k_{Ca} is reduced from the value given in Table 2. This is in qualitative agreement with the observation in Reiser and Matthews (9) that the period grew when the concentration of external Na^+ and subsequently the pump rate of the Na/Ca exchanger was reduced.

We next discuss the bifurcation diagram of our model obtained by using a combination of self-written code and AUTO 2000 (40). Fig. 5 shows the range of values of k_{act}^+ , σ , and $[\text{CaM}^{\text{tot}}]$, respectively, in which the oscillations exist (other parameter values remain as in Table 2). For $\sigma = 0.05$

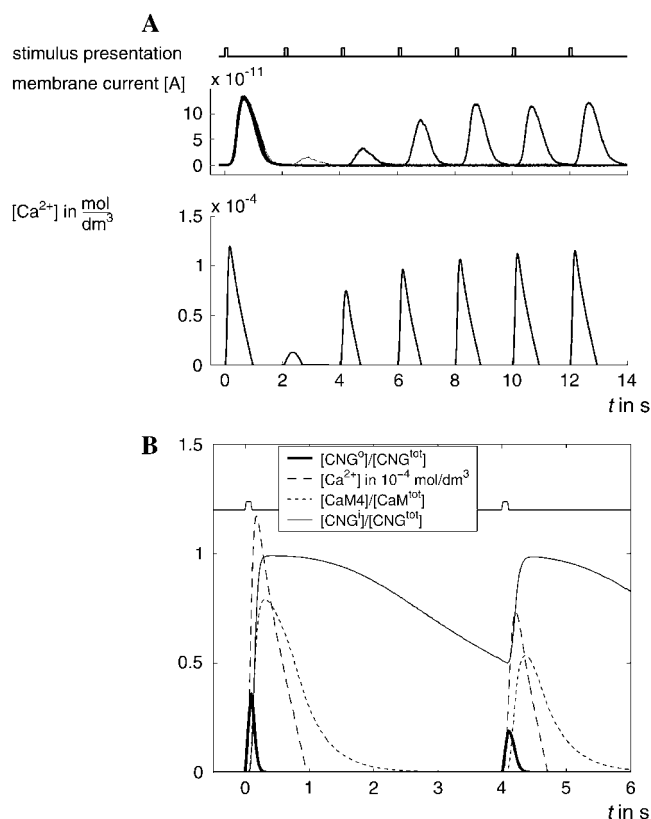


FIGURE 3 (A) Adaptation in double-pulse experiments. The middle row shows the experimental data of Fig. 8 A in Leinders-Zufall et al. (37) (with inverted sign; reprinted with permission). A first pulse at 0 s is followed by a second pulse after 2, 4, 6, 8, 10, and 12 s, respectively, with identical pulse lengths of 100 ms (upper row). The time courses of the membrane current for each pair of pulses are superimposed. The result of our simulation for internal Ca^{2+} concentration is presented in the lower row in the same manner. (B) Time courses of the dynamical variables in the simulation. Except for $[\text{Ca}^{2+}]$, fractions of total concentrations are plotted as indicated in the legend.

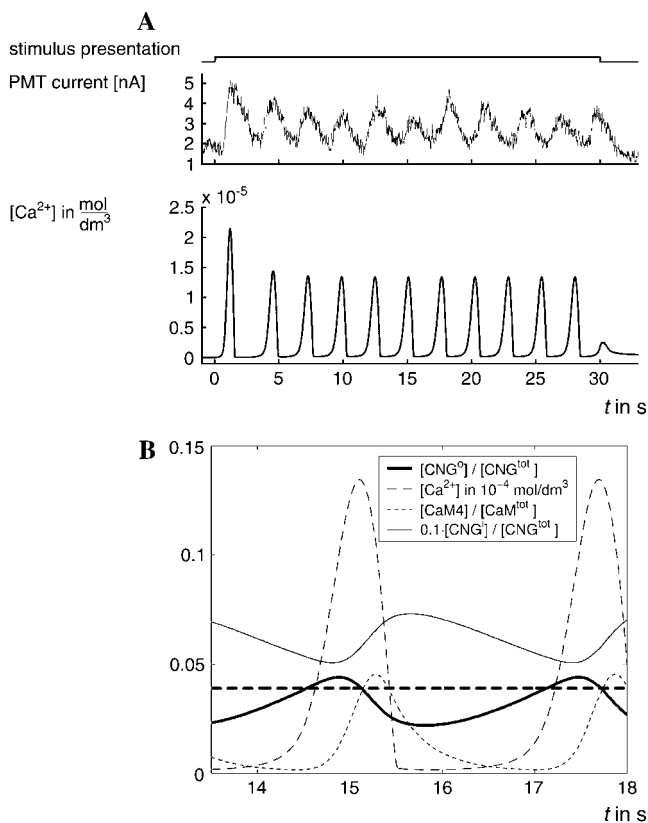


FIGURE 4 (A) Oscillations during prolonged stimulus. The odorant was presented from 0 to 30 s (*upper trace*). The simulation result is presented in the row below. To match experimental conditions the magnitude of the stimulus k_{act}^+ was set (see the main text) to 1% of the value used in Fig. 3. The middle row shows the experimental data of the fluorescence measurements presented in Fig. 5 A in Reisert and Matthews (9) (reprinted with permission). (B) Time courses of the dynamical variables in the simulation. Except for $[Ca^{2+}]$, fractions of total concentrations are plotted as indicated in the legend. The relative fraction $[CNG^i]/[CNG^{tot}]$ is divided by a factor of 10 for convenience of plotting.

μM , the range of stability spans three decades in k_{act}^+ , which (under the assumptions given above), corresponds to a factor of ~ 30 in odorant concentration. This is in agreement with the experiments of Reisert and Matthews (12), in which oscillations were observed for cineole concentrations of 30 μM and 100 μM , but not 10 μM or 300 μM .

Fig. 5 B shows that our results are robust over a wide range of calmodulin concentration. In the shaded area, Ca^{2+} increases without bound. This is a consequence of the minimal assumptions of our model; in reality, the Ca^{2+} current through an open channel i_{Ca} will decay as the internal Ca^{2+} concentration increases. (To adequately describe the dependence of i_{Ca} on $[Ca^{2+}]$, it would be necessary to include the transmembrane voltage V as a dynamical variable of our model. This in turn would require the inclusion of the dynamics of Ca^{2+} -gated chloride channels, making the model significantly more complex and increasing the number of unknown parameters.)

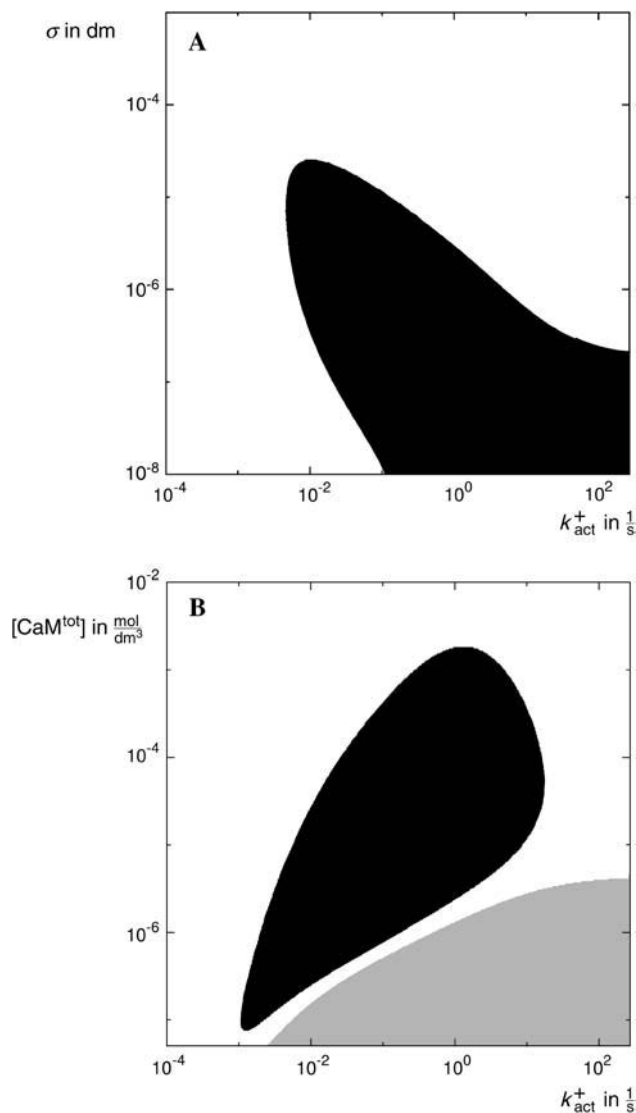


FIGURE 5 Asymptotic behavior of the model as a function of (A) layer thickness σ and (B) total calmodulin concentration $[CaM^{tot}]$ versus the measure of stimulus strength, k_{act}^+ . Black indicates the occurrence of oscillations, white a stable fixed point. In the shaded area in panel B, no fixed point was reached; instead, there was unlimited increase of $[Ca^{2+}]$ (see the main text).

DISCUSSION

The described mechanism is an example of a nonautocatalytic oscillator, i.e., one in which oscillations arise out of a negative feedback loop only, without necessity of destabilizing positive loops. Such oscillators require 1), a negative loop consisting of a considerable number of species with kinetics with about equal timescales; 2), at least one cycle reaction with very high order; or 3), all exit reactions of the cycle of very low order (or a combination of the above). These conditions can be readily generated in abstract models (3,35,41–43), but are rarely found in reality. Circadian rhythms (44,45) and the synthetic system of Elowitz and Liebler (46) provide examples of

oscillations of this type in genetic networks. To our knowledge, no chemical oscillator of this type without enzymes has been identified yet. Typically, nonautocatalytic oscillators differ from autocatalytic ones (i.e., which contain positive feedback) in that they do not give rise to bistability nor excitability.

It is well established that three Ca^{2+} /CaM-mediated feedback loops act in olfactory cilia (see Fig. 1). All three loops can, in principle, lead to adaptation and to oscillations by themselves. In addition to modulating the CNG channel directly, CaM4 accelerates the degradation of cAMP through an enhancement of PDE activity, and reduces the production of cAMP through CaMKII by inhibition of adenylyl cyclase activity. The latter process is known to be quite slow (14) compared to the direct pathway, believed to be responsible for fast adaptation (23). The oscillations (with a period of the order of 1 s) seen in experiment are too fast to be attributable to the cyclase pathway. The timescale on which the PDE pathway operates is expected to be slower than the direct way, since its last step to close the loop involves the detachment of cAMP from the channels and its subsequent degradation. In addition, according to Kurahashi and Menini (17), the effect of PDE on fast adaptation is weak. We conclude that the direct CaM4 feedback is the primary cause for both fast adaptation and oscillation. In principle the interaction of, e.g., the PDE and the direct pathway may give rise to complex oscillations. Also, interaction with CICR is conceivable. Extension of the model to include these effects may become of interest in the future.

The described oscillatory mechanism is expected to manifest itself also in systems other than olfactory sensory neurons. Besides the presence of calmodulin, it requires calcium channels that are negatively regulated by CaM4, Ca^{2+} pumps or exchangers near saturation (which does not exclude that the dominant extrusion mechanisms at Ca^{2+} concentrations outside the oscillatory range are higher-order), as well as confinement to small volumes so that high concentrations of internal Ca^{2+} can be achieved and maintained.

Besides the CNG channels in olfactory cilia, other Ca^{2+} -permeable channels that are strongly inhibited by CaM4 include CNG channels in photoreceptor rods and cones (47), NR1-type NMDA receptors (48), as well as L-type and P/Q-type voltage-dependent channels (49). Our assumption of a well-mixed system will remain reasonably well fulfilled for volume/area ratios σ up to $\approx 1 \mu\text{m}$ (e.g., for cilia and dendrites). For the parameter values used in our model, oscillations persist up to σ beyond this value (up to $5 \mu\text{m}$ in Fig. 5). Thus, any system sufficiently small to fulfill the homogeneity condition will lie well within the oscillatory range. Even for larger systems (e.g., a typical cell), at least transient oscillations may still be observable as the buildup and decay of the concentration gradient near the membrane may drive the system through the oscillatory regime. Including diffusion to describe time-dependent concentration gradients will be one of future extensions of our model.

In cellular compartments with internal Ca^{2+} stores, oscillations can arise based on the autocatalytic calcium-induced

calcium release. A distinguishing feature of the nonautocatalytic mechanism (i.e., a mechanism without positive feedback) is that in contrast to CICR, it does not give rise to excitability and does not support corresponding Ca^{2+} waves. Excitability (i.e., a system makes a large excursion when subjected to a stimulus above a certain threshold before returning to its initial state) requires an autocatalysis to support the self-enhancement of the deviation from steady state. This mechanistic requirement is not fulfilled in a system based solely on negative feedback. Typically, excitable systems exhibit a refractory period (i.e., a certain time has to elapse before the next large excursion can be triggered). The present model shows signs of refractoriness (adaptation) without having the other characteristics of excitability.

APPENDIX: ALTERNATIVE PARAMETER SET

Rate constants reported in the literature on calcium-calmodulin kinetics (36,50–52) vary by up to two orders of magnitude. The numerical results of “Kinetic Model and Numerical Analysis” were obtained using $k_{\text{CaM4}}^+ = 1.1 \times 10^9 (1/\text{s})(\text{dm}^6/\text{mol}^2)$ and $k_{\text{CaM4}}^- = 2.5 (1/\text{s})$ in the effective reaction Eq. 7. With this choice, the calcium-calmodulin binding curve and kinetics resemble those of the model of Bhalla (51) and Sivakumaran et al. (52). Cohen and Klee (36) and Delville et al. (50), however, imply significantly higher values of k_{CaM4}^+ . We therefore examined our model also for k_{CaM4}^+ increased to $2.2 \times 10^{11} (1/\text{s})(\text{dm}^6/\text{mol}^2)$. To obtain adaptation and oscillation dynamics consistent with the experimental data in Figs. 3 and 4, it was then necessary to adjust the values of several other parameters as follows: $[\text{CaM}^{\text{tot}}] = 10^{-5} (\text{mol}/\text{dm}^3)$; $k_{\text{CNG}^o}^- = 2.5 \times 10^{-3} (1/\text{s})$; $k_{\text{CNG}^i}^- = 2.3 \times 10^{-1} (1/\text{s})$; $i_{\text{Ca}} = 8 \times 10^4 (1/\text{s})$; $k_{\text{Ca}} = 8.3 \times 10^{-12} (1/\text{s})(\text{mol}/\text{dm}^2)$; $K_{\text{Ca}} = 8 \times 10^{-9} (\text{mol}/\text{dm}^3)$; $k_{\text{act}}^+ = 1.8 \times 10^{-3} (1/\text{s})$ (oscillations); and $k_{\text{act}}^+ = 1.8 \times 10^{-1} (1/\text{s})$ (adaptation). Other parameters remain as in Table 2. With the new parameter set, the time courses of $[\text{Ca}^{2+}]$ predicted by the model are very similar to the model curves in Figs. 3 and 4; however, the maximum $[\text{Ca}^{2+}]$ values are now $8 \mu\text{M}$ in the adaptation case, and $1 \mu\text{M}$ in the oscillations case. In addition, the oscillatory regions in the state diagrams are now significantly smaller than those with the original parameter set (Fig. 5, A and B). Both parameter sets are consistent with known physiological ranges of rate constants (see Table 2). However, we consider the Ca^{2+} concentrations predicted with the second parameter set to be too low in the case of oscillations, as $1 \mu\text{M}$ of $[\text{Ca}^{2+}]$ is not sufficient to fully activate chloride channels (21).

Note added in proof: We have recently learned of an alternative, and substantially different, mathematical model for adaptation in olfactory cilia by Dougherty et al. (*Proc. Natl. Acad. Sci. USA.*, 102 (2005)). An advantage of our model is that we were able to use the same parameter set to reproduce data for both adaptation and calcium oscillations.

We thank F. Zufall and H.R. Matthews for giving permission to reprint their experimental data, and R. Friedrich, T. Kuner, A. Schäfer, and H. Spors for discussions on olfaction.

J.R. and J.S. thank the Heidelberg Academy of Science and Humanities and the State Baden-Württemberg for financial support.

REFERENCES

- Berridge, M. J., M. D. Bootman, and H. L. Roderick. 2003. Calcium signalling: dynamics, homeostasis and remodelling. *Nat. Rev. Mol. Cell Biol.* 4:517–529.
- Goldbeter, A., and G. Dupont. 1990. Allosteric regulation, cooperativity and biochemical oscillations. *Biophys. Chem.* 37:341–353.
- Rapp, P. E., and M. J. Berridge. 1977. Oscillations in calcium-cyclic AMP control loops form the basis of pacemaker activity and other high frequency biological rhythms. *J. Theor. Biol.* 66:497–525.

4. Cooper, D. M., N. Mons, and J. Karpen. 1995. Adenylyl cyclases and the interaction between calcium and cAMP signalling. *Nature*. 374:421–424.
5. Gorbunova, Y., and N. Spitzer. 2002. Dynamic interactions of cyclic AMP transients and spontaneous Ca^{2+} spikes. *Nature*. 418:93–96.
6. Termonia, Y., and J. Ross. 1982. Entrainment and resonance in glycolysis. *Proc. Natl. Acad. Sci. USA*. 79:2878–2881.
7. Eiswirth, M., A. Freund, and J. Ross. 1991. Operational procedure towards the classification of chemical oscillators. *J. Phys. Chem.* 95: 1294–1299.
8. Firestein, S. 2001. How the olfactory system makes sense of scents. *Nature*. 413:211–218.
9. Reisert, J., and H. R. Matthews. 2001. Simultaneous recording of receptor current and intraciliary Ca^{2+} concentration in salamander olfactory receptor cells. *J. Physiol.* 535:637–645.
10. Frings, S., and B. Lindemann. 1988. Odorant response of isolated olfactory receptor cells is blocked by amiloride. *J. Membr. Biol.* 105:233–243.
11. Reisert, J., and H. R. Matthews. 2001. Responses to prolonged odour stimulation in frog olfactory receptor cells. *J. Physiol.* 534:179–191.
12. Reisert, J., and H. R. Matthews. 2001. Response properties of isolated mouse olfactory receptor cells. *J. Physiol.* 530:113–122.
13. Suzuki, N., M. Takahata, and K. Sato. 2002. Oscillatory current responses of olfactory receptor neurons to odorants and computer simulation based on a cyclic AMP transduction model. *Chem. Senses*. 27:789–801.
14. Wei, J., A. Z. Zhao, G. C. Chan, L. P. Baker, S. Impey, J. A. Beavo, and D. R. Storm. 1998. Phosphorylation and inhibition of olfactory adenylyl cyclase by CaM kinase II in neurons: a mechanism for attenuation of olfactory signals. *Neuron*. 21:495–504.
15. Zufall, F., G. M. Shepherd, and S. Firestein. 1991. Inhibition of the olfactory cyclic nucleotide-gated ion channel by intracellular calcium. *Proc. R. Soc. Lond. B Biol. Sci.* 246:225–230.
16. Chen, T. Y., and K. W. Yau. 1994. Direct modulation by Ca^{2+} -calmodulin of cyclic nucleotide-activated channel of rat olfactory receptor neurons. *Nature*. 368:545–548.
17. Kurahashi, T., and A. Menini. 1997. Mechanism of odorant adaptation in the olfactory receptor cell. *Nature*. 385:725–729.
18. Kelliher, K. R., J. Ziesmann, S. D. Munger, R. R. Reed, and F. Zufall. 2003. Importance of the CNGA4 channel gene for odor discrimination and adaptation in behaving mice. *Proc. Natl. Acad. Sci. USA*. 100: 4299–4304.
19. Bradley, J., D. Reuter, and S. Frings. 2001. Facilitation of calmodulin-mediated odor adaptation by cAMP-gated channel subunits. *Science*. 294:2176–2178.
20. Munger, S. D., A. P. Lane, H. Zhong, T. Leinders-Zufall, K. W. Yau, F. Zufall, and R. R. Reed. 2001. Central role of the CNGA4 channel subunit in Ca^{2+} -calmodulin-dependent odor adaptation. *Science*. 294:2172–2175.
21. Schild, D., and D. Restrepo. 1998. Transduction mechanisms in vertebrate olfactory receptor cells. *Physiol. Rev.* 78:429–466.
22. Reisert, J., P. J. Bauer, K. W. Yau, and S. Frings. 2003. The Ca-activated Cl channel and its control in rat olfactory receptor neurons. *J. Gen. Physiol.* 122:349–363.
23. Zufall, F., and T. Leinders-Zufall. 2000. The cellular and molecular basis of odor adaptation. *Chem. Senses*. 25:473–481.
24. Clarke, B. 1980. Stability of complex reaction networks. *Adv. Chem. Phys.* 43:1–215.
25. Clarke, B. 1988. Stoichiometric network analysis. *Cell Biophys.* 12: 237–253.
26. Epstein, I., and J. Pojman. 1998. An Introduction to Nonlinear Chemical Dynamics, Chapt. 5. Oxford University Press, Oxford, UK.
27. Klamt, S., and E. Gilles. 2004. Minimal cut sets in biochemical reaction networks. *Bioinformatics*. 20:226–234.
28. Klamt, S. 2005. FLUXANALYZER: exploring structure, pathways, and fluxes in (bio)chemical reaction networks. <http://www.mpi-magdeburg.mpg.de/projects/fluxanalyzer>.
29. Gatermann, K. 2001. Counting stable solutions of sparse polynomial systems in chemistry. In *Symbolic Computation: Solving Equations in Algebra, Geometry, and Engineering*, Vol. 286. E. Green, editor. American Mathematical Society, Providence, RI. 53–69.
30. Eiswirth, M., K. Gatermann, and A. Sensse. 2005. Toric ideals and graph theory to analyze Hopf bifurcations in mass action systems. *J. Symbol. Comp.* In press.
31. Eiswirth, M. 1994. *Kagaku ni okeru fuanteisei to shindoo* (Instability and oscillations in chemistry). *Suuri Kagaku*. 372:59–64.
32. Eiswirth, M., J. Bürger, P. Strasser, and G. Ertl. 1996. Oscillating Langmuir-Hinshelwood mechanisms. *J. Phys. Chem.* 100:19118–19123.
33. Clarke, B. 1981. Complete set of steady states for the general stoichiometric dynamical system. *J. Chem. Phys.* 75:4970–4979.
34. Eiswirth, M., A. Freund, and J. Ross. 1991. Mechanistic classification of chemical oscillators and the role of species. *Adv. Chem. Phys.* 80:127–199.
35. Tyson, J. J. 1975. Classification of instabilities in chemical reaction networks. *J. Chem. Phys.* 62:1010–1015.
36. Cohen, P., and C. B. Klee, editors. 1988. *Calmodulin*. Elsevier, Amsterdam, New York.
37. Leinders-Zufall, T., C. A. Greer, G. M. Shepherd, and F. Zufall. 1998. Imaging odor-induced calcium transients in single olfactory cilia: specificity of activation and role in transduction. *J. Neurosci.* 18:5630–5639.
38. Lindemann, B. 2001. Predicted profiles of ion concentrations in olfactory cilia in the steady state. *Biophys. J.* 80:1712–1721.
39. Kleene, S. J. 1999. Both external and internal calcium reduce the sensitivity of the olfactory cyclic-nucleotide-gated channel to cAMP. *J. Neurophysiol.* 81:2675–2682.
40. Doedel, E., R. Paffenroth, A. Champneys, T. Fairgrieve, Y. Kuznetsov, B. Sandstede, and X. Wang. 2001. AUTO 2000: Continuation and bifurcation software for ordinary differential equations (with HOM-CONT). Technical report. Caltech, Pasadena, CA.
41. Goodwin, B. C. 1966. An entrainment model for timed enzyme syntheses in bacteria. *Nature*. 209:479–482.
42. Griffith, J. 1968. Mathematics of cellular control processes. I. Negative feedback to one gene. *J. Theor. Biol.* 20:202–208.
43. Walter, C. 1969. Oscillations in controlled biochemical systems. *Biophys. J.* 9:863.
44. Goldbeter, A. 2002. Computational approaches to cellular rhythms. *Nature*. 420:238–245.
45. Forger, D. B., and C. S. Peskin. 2003. A detailed predictive model of the mammalian circadian clock. *Proc. Natl. Acad. Sci. USA*. 100:14806–14811.
46. Elowitz, M. B., and S. Leibler. 2000. A synthetic oscillatory network of transcriptional regulators. *Nature*. 403:335–338.
47. Burns, M. E., and D. A. Baylor. 2001. Activation, deactivation, and adaptation in vertebrate photoreceptor cells. *Annu. Rev. Neurosci.* 24:779–805.
48. Ehlers, M. D., S. Zhang, J. P. Bernhardt, and R. L. Huganir. 1996. Inactivation of NMDA receptors calmodulin with the NR1 subunit. *Cell*. 84:745–755.
49. Saimi, Y., and C. Kung. 2002. Calmodulin as an ion channel subunit. *Annu. Rev. Physiol.* 64:289–311.
50. Delville, A., P. Laszlo, and D. Nelson. 1985. Calmodulin: calcium, potassium, and magnesium ion multiple equilibria and kinetics for interconversion, including the effect of repeated stimulation. *J. Theor. Biol.* 112:157–175.
51. Bhalla, U. 2005. The database of quantitative cellular signaling. <http://doqs.ncbs.res.in/~doqs/>.
52. Sivakumaran, S., S. Hariharaputran, J. Mishra, and U. Bhalla. 2003. The database of quantitative cellular signaling: management and analysis of chemical kinetic models of signaling networks. *Bioinformatics*. 19:408–415.
53. Larsson, H. P., S. J. Kleene, and H. Lecar. 1997. Noise analysis of ion channels in non-space-clamped cables: estimates of channel parameters in olfactory cilia. *Biophys. J.* 72:1193–1203.
54. Anholt, R. R., and A. M. Rivers. 1990. Olfactory transduction: cross-talk between second-messenger systems. *Biochemistry*. 29: 4049–4054.